Atmos. Chem. Phys., 17, 10245–10258, 2017
https://doi.org/10.5194/acp-17-10245-2017

Atmospheric Chemistry and Physics
Open Access
EGU

Impacts of traffic emissions on atmospheric particulate nitrate and organics at a downwind site on the periphery of Guangzhou, China

Yi Ming Qin[1], Hao Bo Tan[2], Yong Jie Li[3], Misha I. Schurman[4], Fei Li[2], Francesco Canonaco[5], André S. H. Prévôt[5], and Chak K. Chan[1,4,6]

[1]Department of Chemical and Biomolecular Engineering, Hong Kong University of Science and Technology, Hong Kong, China
[2]Key Laboratory of Regional Numerical Weather Prediction, Institute of Tropical and Marine Meteorology, China Meteorological Administration, Guangzhou, China
[3]Department of Civil and Environmental Engineering, Faculty of Science and Technology, University of Macau, Taipa, Macau, China
[4]Division of Environment, Hong Kong University of Science and Technology, Hong Kong, China
[5]Laboratory of Atmospheric Chemistry, Paul Scherrer Institute, 5232, Villigen PSI, Switzerland
[6]School of Energy and Environment, City University of Hong Kong, Hong Kong, China

Correspondence to: Chak K. Chan (chak.k.chan@cityu.edu.hk) and Yong Jie Li (yongjieli@umac.mo)

Received: 7 February 2017 – Discussion started: 15 March 2017
Revised: 14 July 2017 – Accepted: 25 July 2017 – Published: 1 September 2017

Abstract. Particulate matter (PM) pollution on the peripheries of Chinese megacities can be as serious as in cities themselves. Given the substantial vehicular emissions in inner-city areas, the direct transport of primary PM (e.g., black carbon and primary organics) and effective formation of secondary PM from precursors (e.g., NO_x and volatile organic compounds) can contribute to PM pollution in "buffer" zones between cities. To investigate how traffic emissions in inner-city areas impact these adjacent buffer zones, a suite of real-time instruments were deployed in Panyu, downwind from central Guangzhou, from November to December 2014. Nitrate mass fraction was higher on high-PM days, with the average nitrate-to-sulfate ratio increasing from around 0.35 to 1.5 as the PM mass concentration increased from 10 to 160 $\mu g\,m^{-3}$. Particulate nitrate was strongly correlated with excess ammonium ($([NH_4^+]/[SO_4^{2-}]-1.5)\times[SO_4^{2-}]$), with higher concentrations in December than in November due to lower temperatures. The organic mass fraction was the highest across all PM_1 levels throughout the campaign. While organic aerosols (OA) were dominated by secondary organic aerosols (SOA = semi-volatile oxygenated organic aerosols + low-volatility oxygenated organic aerosols) as a campaign average, freshly emitted hydrocarbon-like organic aerosols (HOA) contributed up to 40 % of OA during high-OA periods, which typically occurred at nighttime and contributed 23.8 to 28.4 % on average. This was due to daytime traffic restrictions on heavy-duty vehicles in Guangzhou, and HOA almost increased linearly with total OA concentration. SOA increased as odd oxygen ($O_x = O_3 + NO_2$) increased during the day due to photochemistry. A combination of nighttime traffic emissions and daytime photochemistry contributed to the buildup of PM in Panyu. The mitigation of PM pollution in inner-city areas by reducing vehicular traffic can potentially improve air quality in peripheral areas.

1 Introduction

Traffic emissions are one of the main contributors to air quality deterioration in rapidly expanding urban China (Kelly and Zhu, 2016; Zhang et al., 2017). Pollutants emitted from vehicles – such as NO_x, volatile organic compounds (VOCs), black carbon (BC) and other traffic-related particulate matter (PM) – have increased over the last decades (Wang et al., 2013; Zhang et al., 2012). Apart from the primary PM, the oxidation of traffic-related gaseous pollutants such as NO_x, VOCs, semi-volatile VOCs (SVOCs) and low-volatility VOCs (LVOCs) leads to the formation of particu-

late nitrate and secondary organic aerosols (SOA), exacerbating PM pollution. Multiple studies have shown that the concentrations and proportions of nitrate in PM have increased significantly in most Chinese megacities (Pan et al., 2016; Wen et al., 2015; Xue et al., 2014).

The rapid economic development in the Pearl River Delta (PRD) region has led to a rapid deterioration in air quality, especially due to a sharp increase in PM (Chan and Yao, 2008; Ho et al., 2003; Li et al., 2017). With densely populated cities including two megacities, Guangzhou and Shenzhen, and other smaller cities, the PRD region is developing into a giant city cluster. There are, nevertheless, less populated areas between these cities that can serve as a "buffer" zone in terms of regional air quality. Due to air dispersion patterns and regulatory strategies, air pollutants in highly urbanized regions can greatly influence PM levels in peripheral regions. For example, highly polluting vehicles such as heavy-duty diesel trucks are banned from the inner areas of many Chinese megacities during the day but are nevertheless active at night and in the early morning, especially on the peripheries of these megacities. This regulatory policy has resulted in nighttime peaks in vehicular pollutants, which have been commonly observed in many Chinese cities (Zhang and Cao, 2015). Although vehicle emissions are substantially reduced relative to the without-control scenarios, there was still significantly higher emission density in east China than in developed countries with longer histories of vehicle emission control (Wu et al., 2016). Given the complex and nonlinear processes involved in the secondary production of PM such as nitrate and organic aerosols, the impacts of these adjacent buffer zones on air quality are crucial. However, relatively little attention has been paid to how air pollutants in major cities affect these adjacent areas.

Panyu district lies directly south of central Guangzhou and experiences predominantly northerly/northeasterly winds between September and February (Zou et al., 2015). A campaign with a host of real-time instruments including an Aerodyne High-Resolution Time-of-Flight Aerosol Mass Spectrometer (HR-ToF-AMS) was conducted at a site in Panyu from November to December 2014 and provides a unique opportunity to explore how pollutants from the city center have impacted this adjacent buffer zone, especially in terms of nitrate and secondary organic aerosols. As will be shown, the mass fraction of nitrate increased as PM_1 increased, and the organic mass fraction was the highest among PM_1 species across all PM_1 levels. A comprehensive analysis of nitrate and organics and their interplay with meteorological parameters will be presented. Primary OA (POA; e.g., hydrocarbon-like organic aerosols (HOA)) and SOA from traffic-related VOC precursors will also be discussed. Our findings can provide useful information for regional emission control strategies covering urban and buffer areas and improving parameterization in air quality models.

2 Method

2.1 Sampling site description

Guangzhou Panyu Atmospheric Composition Station (GPACS), a China Meteorological Administration site, is located at the summit of Dazhengang (23°00 N, 113°21 E) at an altitude of approximately 150 m (Fig. S1 in the Supplement). The site is approximately 15 km south of the city center and surrounded by residential neighborhoods with no significant industrial sources nearby (Tan et al., 2013; Cheung et al., 2016). Ambient sampling was conducted from 7 November 2014 to 3 January 2015.

2.2 Measurements

In the HR-ToF-AMS measurements (DeCarlo et al., 2006), ambient air was sampled through a $PM_{2.5}$ cyclone on the rooftop with a flow rate of approximately $0.084\,L\,min^{-1}$ drawn by the AMS and the remainder drawn by an auxiliary pump. A diffusion drier was used to dry the sampled air stream, which reduced the relative humidity (RH) of the air to below 30 % before entering the HR-ToF-AMS. Other data presented in this work were obtained from collocated instruments including a Grimm 180 for $PM_{2.5}$, a thermo-optical elemental carbon and organic carbon (ECOC) analyzer (Sunset Laboratory Inc.), a Magee Aethalometer Model AE33, a dual-spot filter-based instrument for black carbon (Drinovec et al., 2015), a gas analyzer system (Teledyne Instruments), and a monitor for aerosols and gases in ambient air (MARGA, Metrohm Applikon) with a $PM_{2.5}$ cutoff. The $PM_{2.5}$ mass concentration as measured with a Grimm 180 was corrected using the daily $PM_{2.5}$ mass concentration through quartz filter measurement (Sect. S1 in the Supplement). Meteorological data (e.g., wind, temperature and RH) were obtained from a weather station located near the sampling site. Solar irradiance data were measured from a station in Nansha district, around 27.5 km from the sampling site. Particle liquid water content (LWC) was estimated with an aerosol inorganic model (E-AIM II) (Clegg et al., 1998).

The AMS collected 5 min average particle mass spectra spanning from m/z 12 to 300 for the V+ particle time-of-flight (pToF) mode (high sensitivity) and the W mode (high resolution). The high-resolution mode only analyzed the signals with m/z below 200. AMS calibrations – including ionization efficiency (IE) calibration, flow rate calibration and size calibration – were used as well as data quality assurance protocols (DeCarlo et al., 2006; Lee et al., 2013; Schurman et al., 2015). IE calibrations with differential mobility analyzer (DMA) size-selected (mobility diameter, $D_m = 400$ nm) pure ammonium nitrate particles were carried out weekly. Ambient air filtered with a HEPA filter was sampled on a daily basis for 30 min to obtain background signals. Flow rate calibrations were made with a Gilian Gilibrator. PToF size calibrations were made with Nanosphere

TM polystyrene latex spheres (PSL) particles (Duke Scientific, Palo Alto, CA, USA) and ammonium nitrate particles in the size range of 178 to 800 nm (selected with a DMA). Both flow rate and size calibrations were performed before and after the sampling campaign. Gaseous CO_2 concentrations were measured with a CO_2 monitor (PICARRO 2301) and were used to correct their contributions to m/z 44 signal intensities.

2.3 Data analysis

AMS data analysis was performed using the SQUIRREL (v1.56D) and PIKA (v1.15D) toolkits written in Igor Pro 6.37A (WaveMetrics Inc., Lake Oswego, OR, USA). Default relative ionization efficiency (RIE) values of 1.2 for sulfate, 1.1 for nitrate, 1.3 for chloride and 1.4 for organics were used. The ammonium RIE of 4.7 was chosen as the average from IE calibrations. A particle collection efficiency factor (CE) of 0.7 was used to account for particle losses within the instrument. The influence of RH in this study was minor, as a diffusion drier was used to maintain the sampling line RH consistently below 30 %. Under these conditions, Middlebrook's parameterization suggests a CE of ∼ 45–50 % based on the measured inorganic constituents (Middlebrook et al., 2012). However, organic compounds, which are less bouncy than inorganics, dominated at the measurement site. They can also hinder the complete efflorescence of particles in the drier and further reduce the particle bounce effect and increase particle collection efficiency. The mass concentrations of PM_1 (sum of nonrefractory PM_1 and BC) were comparable to those of $PM_{2.5}$ with a slope of 1.1 and Pearson's correlation coefficient (R_p) of 0.95 (Fig. S2a) when using a CE of 0.7. Furthermore, total AMS organics were also correlated with organic matter (OM) concentrations derived from the OC measurements (Fig. S2b) with a slope of 1.1 and R_p of 0.82. The OC-to-OM conversion was calculated using organic-matter-to-organic-carbon ratio (OM : OC) data from the HR-ToF-AMS elemental analysis. AMS-measured sulfate, nitrate and ammonium were comparable to those measured with MARGA with slopes of 1.0, 0.9 and 0.7, respectively. These comparisons suggest that a choice of CE = 0.7 is appropriate for the OA-dominating nonrefractory PM_1 (NR-PM_1) in this study.

Source apportionment for OA was performed using the newly developed Multilinear Engine (ME-2) via the SoFi interface coded in Igor Pro (Canonaco et al., 2013). The procedure allows an effective exploration of the solution space, a more objective selection of the optimal solution and an estimation of the rotational uncertainties (Canonaco et al., 2013; Crippa et al., 2014; Elser et al., 2016; Fröhlich et al., 2015; Paatero and Hopke, 2009). We only considered ions up to m/z 100 due to the low signal-to-noise ratios of larger ions. Fully unconstrained runs (as in traditional PMF analysis) were first explored. However, the three-factor solution suffers from the mixing of the HOA factor with the cooking organic aerosols (COA) factor (Fig. S4) as well as the semi-volatile oxygenated organic aerosol (SVOOA) factor with the biomass-burning-related organic aerosols (BBOA) factor. The four-factor solution splits highly oxidized low-volatility OOA (LVOOA) into two sub-factors (Fig. S5). The inclusion of additional factors still cannot resolve pure primary OA factors (HOA, COA and BBOA) as they may have similar time series or profiles. Zhang et al. (2013) also reported that the principal-component-analysis-resolved HOA can be affected by cooking emissions with a distinct noontime peak in Beijing in spring and summer. By introducing a priori information of source profiles for HOA, COA and BBOA, the ME-2 provides additional control over the rotational ambiguity (Canonaco et al., 2013; Paatero and Hopke, 2009). The a value, ranging from zero to unity, stands for the extent to which each m/z signal of the final solution spectra may differ from the anchor. A value of 0 means no deviation is allowed, while a value of 1 means 100 % deviation is allowed.

The OA source apportionment was performed by constraining the source profile of HOA, COA and BBOA with a values of 0.1, 0.2 and 0.3 for HOA, COA and BBOA, respectively. The HOA source profile was extracted from the data set using a separate PMF run in selected time series with peaks in organic mass concentration. The COA reference was adopted from the Mong Kok campaign in Hong Kong (Lee et al., 2015), while the reference BBOA profile was adopted from MILAGRO (Aiken et al., 2009). A detailed discussion can be found in the Supplement (Sect. S2).

3 Results and discussion

3.1 Overall composition

Northerly winds prevailed throughout the entire campaign (Sect. S3). Located south of central Guangzhou, the sampling site was thus severely affected by pollutants transported from the city center. Overall, organics accounted for 46.3 % (or 24.5 $\mu g\,m^{-3}$) of the PM_1 mass on average. Sulfate, nitrate, ammonium, BC and chloride accounted for 23.1, 11.2, 9.1, 8.3 and 1.9 % of the PM_1 mass, respectively (Fig. 1a). Figure 1b shows the variations in species mass fractions in PM_1 species as a function of total PM_1 mass loading (with BC inclusive) and the probability density of PM_1 mass loading. The organic mass fraction was the highest among all PM_1 species across all PM_1 levels. However, the mass fraction of sulfate decreased from 0.25 to 0.15 as the PM_1 concentration increased from 10 to 160 $\mu g\,m^{-3}$. The decrease in the sulfate mass fraction was compensated for by the increased mass fraction of nitrate and, to a lesser extent, chloride. The mass ratio of nitrate to sulfate in ambient aerosols can be further used to evaluate the relative importance of stationary and mobile sources (Arimoto, 1996; Tan et al., 2009). In our study, the average nitrate-to-sulfate ratios were around

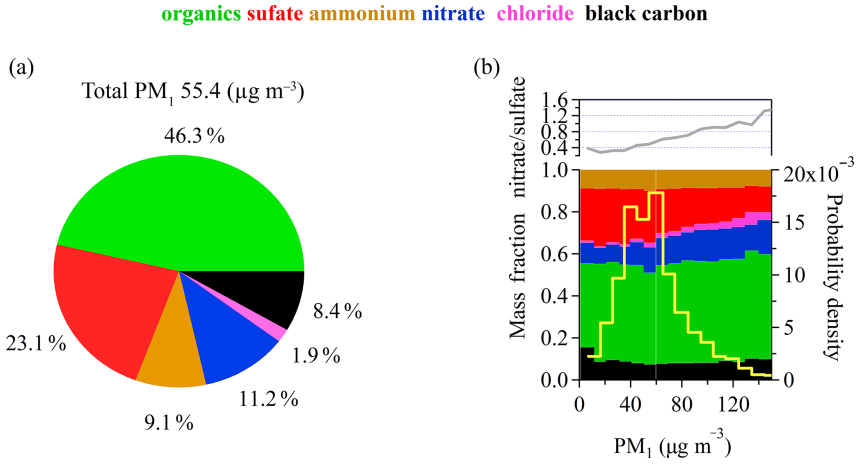

Figure 1. (a) Average mass fraction of PM_1 (with BC inclusive) throughout the entire campaign. **(b)** Mass fraction variation among PM_1 species, nitrate-to-sulfate mass ratio and the probability density of PM_1 as a function of total PM_1 mass loading. The probability density distribution describes the relative likelihood of PM_1 mass loading in a range of concentrations.

0.35 when PM_1 levels were lower than $40\,\mu g\,m^{-3}$. These ratios increased significantly as the PM concentration increased, reaching 1.5 on the highest-PM_1 days (averaging $160\,\mu g\,m^{-3}$), highlighting the substantial contribution of vehicle emission pollutants to PM on high-PM days.

3.2 Nitrate formation

The increase in the relative contribution of nitrate on highly polluted days has also been observed in AMS studies at other locations in China, such as Shenzhen (He et al., 2011), Beijing (Huang et al., 2010) and Changdao (Hu et al., 2013). We used the molar concentration of total nitrate $[HNO_3(g) + NO_3^-(p)]$ to examine the increase in nitrate species, where $HNO_3(g)$ was measured with MARGA and $NO_3^-(p)$ was measured with HR-ToF-AMS. Organic nitrates can show fragments (NO^+ and NO_2^+) similar to inorganic nitrate in HR-ToF-AMS and contribute to the nitrate concentration measured with AMS. Farmer et al. (2010) have used NO^+/NO_2^+ ratios to estimate organic nitrate concentration from HR-ToF-AMS measurements. Xu et al. (2015) suggested using the NO^+ / NO_2^+ values of 5 and 10, which likely correspond to the lower and upper values of the NO^+/NO_2^+ ratio of organic nitrate, to estimate the upper and lower bounds of organic nitrate concentrations. We adopt the NO^+ / NO_2^+ method (hereinafter Method 1) in this study to estimate the contributions of inorganic and organic nitrates. However, the vast array of possible organic nitrate parent compounds in ambient particles and the variations in the NO^+ / NO_2^+ ratios between instruments can lead to biases in the calculations. The organic nitrate concentration can also be estimated using the organic concentration and elemental ratios (OM : OC and N : C) from HR-ToF-AMS measurements (Method 2) (Schurman et al., 2015). Using these two methods (see details in Sect. S4), the contribution from

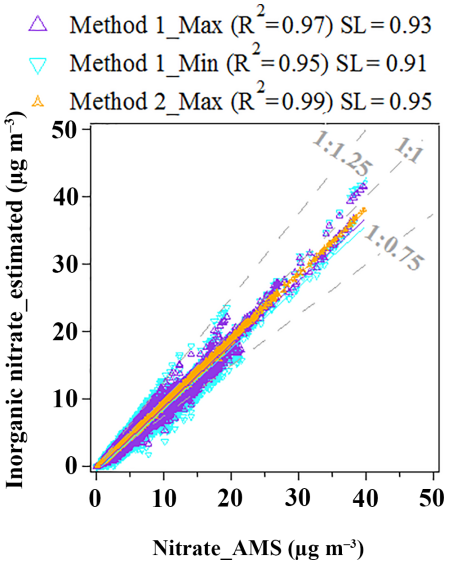

Figure 2. Scatterplot of estimated inorganic nitrate versus nitrate from HR-ToF-AMS measurement. SL denotes the slope for the linear regression fitting.

organic nitrate ranged from around 10 to 25 % of the total AMS-measured nitrate. In Fig. 2, the estimated inorganic nitrate tracked well ($R_p^2 \geq 0.95$, $0.9 < \text{slope} < 1$) with the total HR-ToF-AMS nitrate concentration, closely followed the 1 : 1 line, and mostly lay in the range of the 1 : 1.25 and 1 : 0.75 lines. Furthermore, as shown in Fig. S2, concentrations of nitrate from AMS were comparable to those from MARGA, with a correlation slope of 0.9 and an R_p of 0.95. The influence of organic nitrates in our calculation of total nitrate is expected to be minor. Given the uncertainties associated with each estimation, we use the HR-ToF-AMS nitrate concentration in the following discussions.

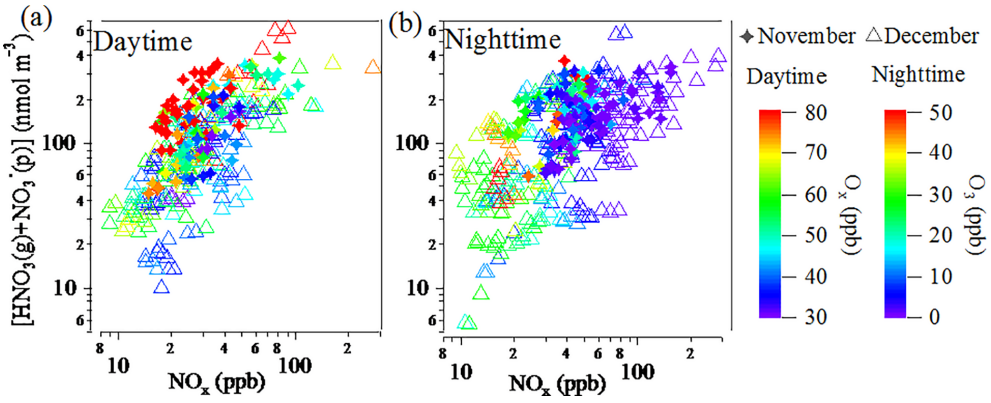

Figure 3. Correlations between total nitrate ($HNO_3(g) + NO_3(p)$) and NO_x ($NO + NO_2$). Triangles and circles represent data for November and December, respectively. Data are color-coded by O_x during the day and O_3 at night.

In Fig. 3, the total (particle + gas) nitrate is closely correlated with NO_x during both daytime and nighttime. At the same NO_x levels, total nitrate increased as O_x increased during the day (Fig. 3a), suggesting the photochemical formation of nitrate. Odd-oxygen ($O_x = O_3 + NO_2$) concentrations are closely linked to the extent of photochemical oxidation in an air mass. We used O_x instead of O_3 to account for the titration of O_3 by freshly emitted NO, which produces NO_2. At night, O_3 concentrations were relatively low when NO_x concentrations were high (Fig. 3b). The slope of total nitrate against NO_x during the day is steeper than that at night. The nighttime formation of nitric acid involves the consumption of NO_x and O_3 (Seinfeld and Pandis, 2006). While NO_x can be replenished by primary emissions, O_3 is mainly produced during the day and consumed at night. Thus high total nitrate concentrations were correlated with high NO_x and low O_3 levels at night.

Gas-to-particle partitioning of nitrate species to form particulate nitrate can be affected by concentrations of ammonium and sulfate. An increase in ammonium or a decrease in sulfate can facilitate the formation of particulate nitrate (Seinfeld and Pandis, 2006). A number of studies have indicated that a molar ratio of ammonium to sulfate of 1.5 demarcates the observation of particulate nitrate (Griffith et al., 2015; Huang et al., 2011a; Liu et al., 2015b; Pathak et al., 2004). Under ammonium-rich (AR, $[NH_4^+] / [SO_4^{2-}] > 1.5$) conditions, additional ammonia is available to transfer HNO_3 to the particle phase. In contrast, under ammonium-poor (AP, $[NH_4^+] / [SO_4^{2-}] < 1.5$) conditions, all of the ammonia is used to neutralize H_2SO_4 until letovicite ($(NH_4)_3H(SO_4)_2$) is formed. AR conditions prevailed throughout the entire campaign. Figure 4 shows that excess ammonium, defined as $([NH_4^+] / [SO_4^{2-}] - 1.5) \times [SO_4^{2-}]$), tracked well with particulate nitrate concentration with a slope of 0.93 and a Pearson's R (R_p) of 0.96. We also found that excess ammonium tracked better with nitrate than Na^+ and Ca^{2+} did (Fig. S16). The slope of nitrate to excess ammonium was less than 1 (Fig. 4), indicating that ammonium was sufficient to neutralize the particulate nitrate. Organic acids and other unmeasured anions may account for the extra ammonium not associated with nitrate. The molar concentrations of alkali cations were around 7–10 times lower than that of nitrate, and their role in stabilizing nitrate was negligible in our study (Fig. S16).

The partitioning of nitrate between the gas and particle phases shows significant differences between November and December (Fig. 5). The average ratio of nitrate to HNO_3 (the slope of the scatterplot) was 3.2 in November and 7.8 in December. NH_3 concentration in the gas phase was not a limiting factor as the concentration of NH_3 was even higher in November than in December (Fig. 5a). Lower temperatures in December shifted the equilibrium toward the particle phase, increasing the nitrate concentration in the particle phase (Fig. 5b). Higher RH or particle liquid water content favors the formation of nitrate, but the effects were not obvious (Fig. 5c, d).

In summary, the NO_x emissions led to nitrate formation during both daytime and nighttime. The fraction of nitrate increased and compensated for the decrease in the fraction of sulfate as the PM_1 concentration increased. Ammonium-rich conditions prevailed, and particulate nitrate tracked well with excess ammonium. Lower temperature in December favors the partitioning of nitrate toward particle phase as compared to November.

3.3 Organics

Organics contributed most to the PM_1 mass measured in Panyu. A growing number of studies have shown that vehicle emissions are important sources of both primary and secondary organic aerosols (Deng et al., 2017; Louie et al., 2005; Platt et al., 2014). Reactive tracer gases and the primary organic pollutants can be oxidized to form SOA in urban air outflows (Gentner et al., 2017).

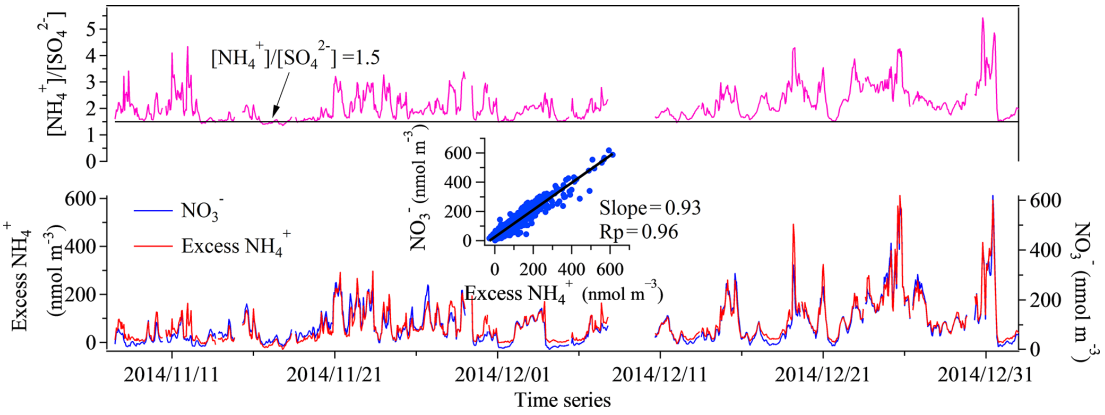

Figure 4. Time series of nitrate, excess ammonium and ammonium-to-sulfate molar ratio.

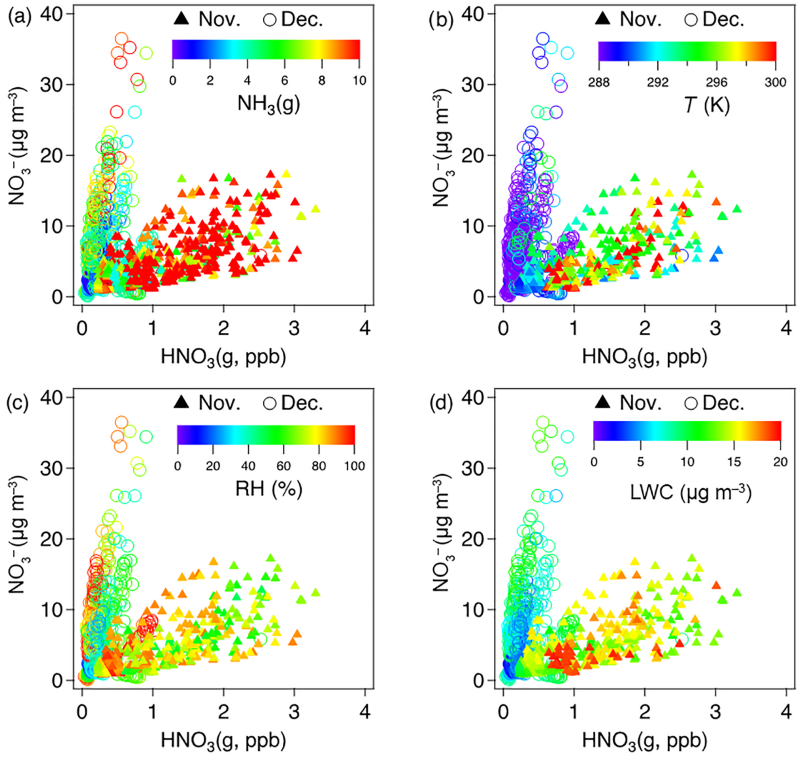

Figure 5. Distribution of nitrate species between HNO_3(g) and NO_3^-(p), colored by **(a)** NH_3 concentration, **(b)** temperature, **(c)** RH and **(d)** LWC.

3.3.1 Elemental analysis of OA

Elemental analysis of OA (ratios of H : C, O : C and OM : OC) provides useful information for assessing OA characteristics and their evolution. Ions in the high-resolution mass spectra were used to calculate the elemental ratios using the improved-ambient method (Canagaratna et al., 2015). Results obtained from the Aiken-ambient (Aiken et al., 2007) protocol are also listed in Table 1 for comparison with elemental ratios reported in the literature. We further used empirical constants (11 % for H : C, 27 % for O : C and 9 % for OM : OC) from Canagaratna et al. (2015) to estimate the ratios accounting for the possible underestimation of the O : C ratio in earlier studies.

The average O : C, H : C and OM : OC ratios showed little variation between the 2 months, with average values of 0.53, 1.63 and 1.87, respectively, in November, and 0.53, 1.65 and 1.87, respectively, in December. The observed elemental ratios generally agreed with other AMS-based reported values in the PRD (Table 1). The H : C ratio was similar to those at rural sites in Kaiping (1.64) and Heshan (1.65) and slightly higher than that in suburban Hong Kong (1.54 and 1.55) but

Table 1. Elemental ratios of organic PM_1 in the PRD.

Site/characteristics	Month	Aiken-ambient (A-A) method			Improved-ambient (I-A) method			Reference
		O : C	H : C	OM : OC	O : C*	H : C*	OM : OC*	
Panyu/suburban	November	0.42	1.49	1.71	0.53	1.63	1.87	This study
	December	0.41	1.5	1.70	0.53	1.65	1.87	
Kaiping/rural	November	0.47	1.48	1.77	0.60*	1.64*	1.94*	Huang et al. (2011)
Shenzhen/urban	November	0.3	1.63	1.57	0.38*	1.81*	1.66*	He et al. (2011)
Heshan/rural	November	0.4	1.49	1.72	0.51*	1.65*	1.83*	Gong et al. (2012)
HKUST/suburban	February	0.42	1.39	1.71	0.53*	1.54*	1.86*	Li et al. (2015)
	December	0.43	1.4	1.71	0.55*	1.55*	1.87*	
Mong Kok/urban	March–mid-May	0.25	1.68	1.49	0.32	1.84	1.59	Lee et al. (2015)

* Improved-ambient elemental ratios were estimated using the A-A method with empirical constants from Canagaratna et al. (2015).

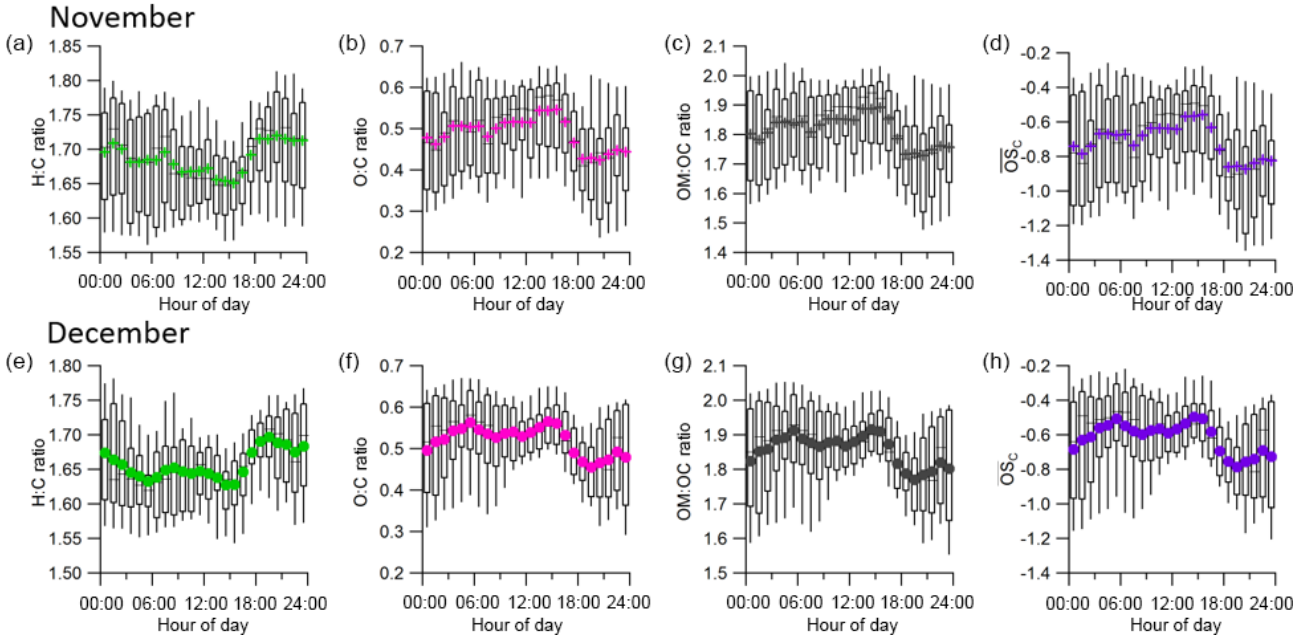

Figure 6. Diurnal variations in H : C **(a, e)**, O : OC **(b, f)** and OM : OC **(c, g)** ratios, and carbon oxidation state ($\overline{OS_c} \approx 2 \times O:C - H:C$) **(d, h)** during November **(a–d)** and December **(e–h)** (25th- and 75th-percentile boxes, 5th- and 95th-percentile whiskers, median as line in box and mean as solid colored line).

lower than those at urban sites in Shenzhen (1.81) and Mong Kok in central Hong Kong (1.84). O : C and OM : OC ratios, however, were higher than those at urban sites (Shenzhen and Mong Kok) and lower than that in Kaiping but similar to those in Heshan and suburban Hong Kong. Overall, the relatively low H : C ratio and high O : C ratio suggest that OA at this site have a higher degree of oxygenation than those at urban sites (e.g., Shenzhen) but a lower degree than those at rural sites (e.g., Kaiping). Figure 6 shows that the diurnal variations in H : C, O : C, OM : OC and carbon oxidation state ($\overline{OS_c} \approx 2 \times O:C - H:C$) were similar in November and December. The average H : C ratio ranged from 1.6 to 1.7, with a pronounced increase in the late afternoon from 16:00 to 20:00 LT (local time), and remained at a maximum until midnight due to fresh organic sources at night. The O : C and OM : OC ratios and $\overline{OS_c}$ increased during the day with afternoon peaks at around 15:00 LT, likely due to high photochemical activity and the production of SOA during daylight hours.

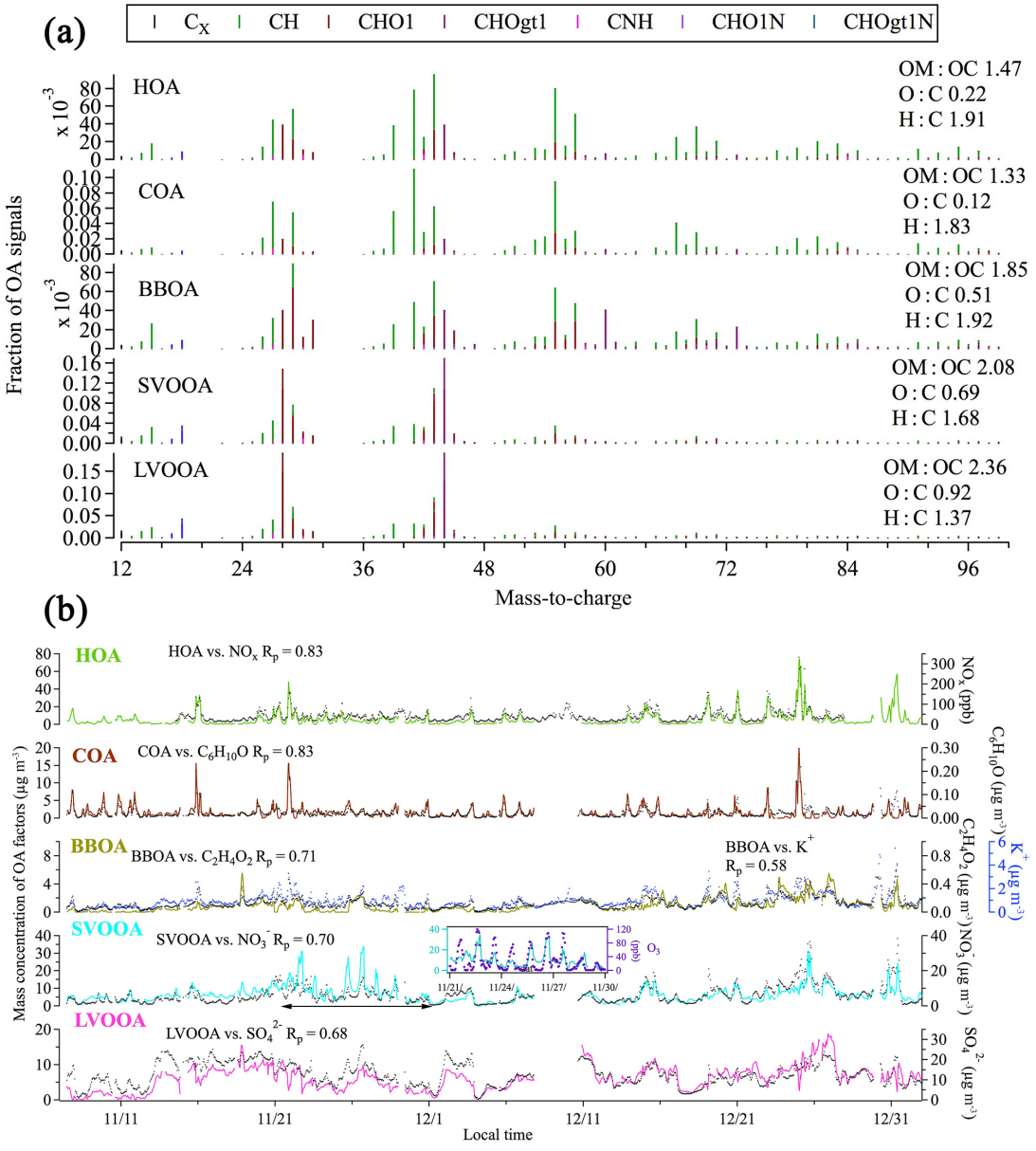

Figure 7. The mass spectra of all OA factors **(a)** and the time series **(b)** of their mass concentrations together with external tracers.

3.3.2 Sources and formation of OA

The mass spectra of all OA factors and their mass concentrations obtained through PMF analysis with ME-2, together with the time series of external tracers, are shown in Fig. 7. HOA correlated well with NO_x since both are traffic-related species. While the mass spectrum of COA shares spectral similarities with that of HOA, it is distinguished by a higher contribution of $C_3H_3O^+$ at m/z 55 and a much lower contribution of ions at m/z 57 (He et al., 2010; Mohr et al., 2012). The time series of COA tracked well with one of its tracer ions, $C_6H_{10}O^+$. The other primary factor, BBOA, is characterized by the presence of signals at m/z 60 ($C_2H_4O_2^+$) and m/z 73 ($C_3H_5O_2^+$), which are typically associated with levoglucosan (Alfarra et al., 2007; Schneider et al., 2006). The time series of COA and BBOA also tracked well with those of their marker ions. The two oxygenated organic aerosol factors (SVOOA and LVOOA) are characterized by oxygenated ions $C_2H_3O^+$ at m/z 43 and CO_2^+ at m/z 44, respectively. The ratio of the most-oxidized ions CO_2^+ (m/z 44) to moderately oxygenated ions $C_2H_3O^+$ (m/z 43) is higher in LVOOA than in SVOOA (Jimenez et al., 2009). Overall, a strong correlation between concentrations of SVOOA and nitrate was observed. Particulate nitrate also represents semi-volatile secondary species, which share similarity with SVOOA in terms of volatility and its partitioning behav-

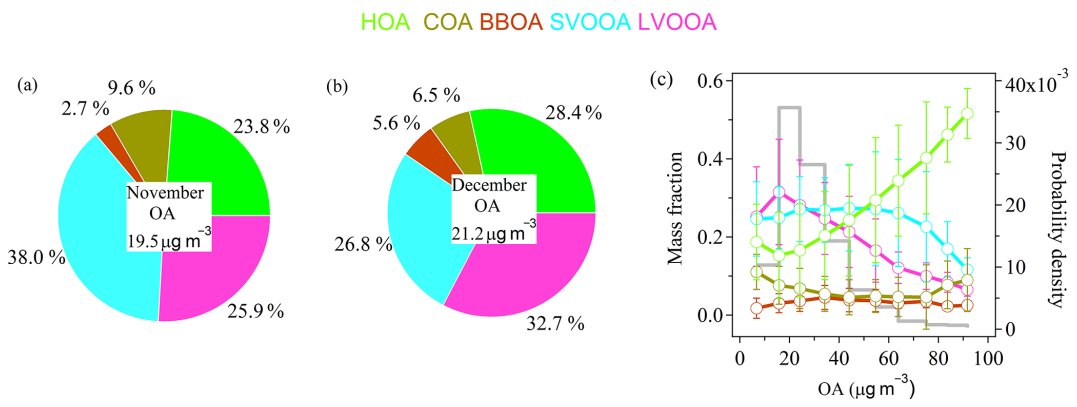

Figure 8. Monthly averages of OA fraction as well as variations in OA fractions in different ranges of OA concentration.

ior with temperature. Such a correlation is widely used in AMS studies (Crippa et al., 2014; Zhang et al., 2011). From 21 November to 1 December (highlighted by the arrow in Fig. 7b), SVOOA showed distinct peaks beyond the comparable trend with nitrate. The sharp peaks of SVOOA coincide with those of O_3, as shown in the inserted panel. Moreover, higher temperatures were also observed during this period (Fig. S5). LVOOA also correlated well with sulfate in time series as both species are regional pollutants.

Figure 8 shows the monthly average of OA fractions as well as their variations in different ranges of OA concentrations. HOA contributed 23.8 % and 28.4 % to total OA in November and December, respectively. However, HOA increased almost linearly with OA concentration, highlighting the need for traffic control to mitigate high PM concentrations in buffer areas. SVOOA and LVOOA remained the dominated OA fractions at OA concentrations below 70 $\mu g\,m^{-3}$, which explains the relatively low HOA contribution on a monthly basis.

Figure 9 shows the diurnal patterns of mass concentrations and fractions for the five OA factors. HOA exhibited two typical peaks in both November and December during the morning rush hour at 09:00 LT and in the evening around 21:00 LT. HOA accounted for up to 40 % of OA (95th percentile of mass fraction in a box-and-whisker plot) especially in the evening and at night, likely due to heavily polluting trucks passing by en route to the city center at night (22:00 to 07:00 LT). These diurnal variations in HOA correspond to those in the H : C ratio and NO_x as well as BC (Fig. S12), further confirming that vehicle-related pollutants are the main contributor to this OA factor. SVOOA had a clear noon-to-afternoon peak in November, consistent with peaks in ozone (Fig. S12), but this peak was less pronounced in December. The noon-to-afternoon peak for SVOOA due to photochemical oxidation processes has been commonly observed worldwide (e.g., Hayes et al., 2013; Qin et al., 2016). It is worthwhile to conduct further study on vehicle-related organic emissions to SVOOA formation. For example, combining radiocarbon and ECOC measurements with the AMS and organic marker measurements, Zotter et al. (2014) found that the noon-to-afternoon SVOOA peak can be attributed to the large increase in fossil OC in the measurements in Pasadena, California, US. LVOOA showed a relatively flat diurnal pattern, as was found in Shenzhen (He et al., 2011), in contrast to the significant noon-to-afternoon peaks for LVOOA at rural sites in Kaiping (Huang et al., 2011b) and Heshan (Gong et al., 2012).

The evolution of AMS OA factors has been used to infer SOA formation via photochemical oxidation in a nearby city, Hong Kong (Lee et al., 2013; Li et al., 2013; Qin et al., 2016). Figure 10 shows that SOA (SVOOA + LVOOA) increased as O_x increased during the day (07:00 to 18:00 LT) in both November and December. The SOA concentrations do not show clear correlations with temperature or liquid water content in aerosols (Fig. S17a, b). When taken together, these observations suggest that SOA formation in our study was dominated by gas-phase oxidation chemistry rather than heterogeneous or aqueous oxidation pathways. Furthermore, the regression slopes for SOA versus O_x are 0.23 ± 0.014 ($R_{pr} = 0.85$) and 0.25 ± 0.025 ($R_{pr} = 0.55$) $\mu g\,(sm^3\,ppb)^{-1}$ for November and December, respectively. The volume unit "sm" stands for volume under standard-temperature-pressure conditions. The slopes are higher than those reported in earlier studies during spring and summer in North America (Table 2), and significant production of SOA may be attributed to the photooxidation of large amounts of accumulated VOCs between the inner city and this peripheral site in Panyu. Liu et al. (2015a) investigated SOA formation from light-duty gasoline vehicles operated in China using a smog chamber under idling conditions. They found that SOA formation was 12–259 times higher than POA under conservative OH exposure. Deng et al. (2017) also revealed that the emission factors for BC and POA from major diesel vehicle types in China under idling conditions and the production factor for SOA under photochemical aging were significantly higher than those in studies in Europe and the US and those from light-duty gasoline vehicles in China.

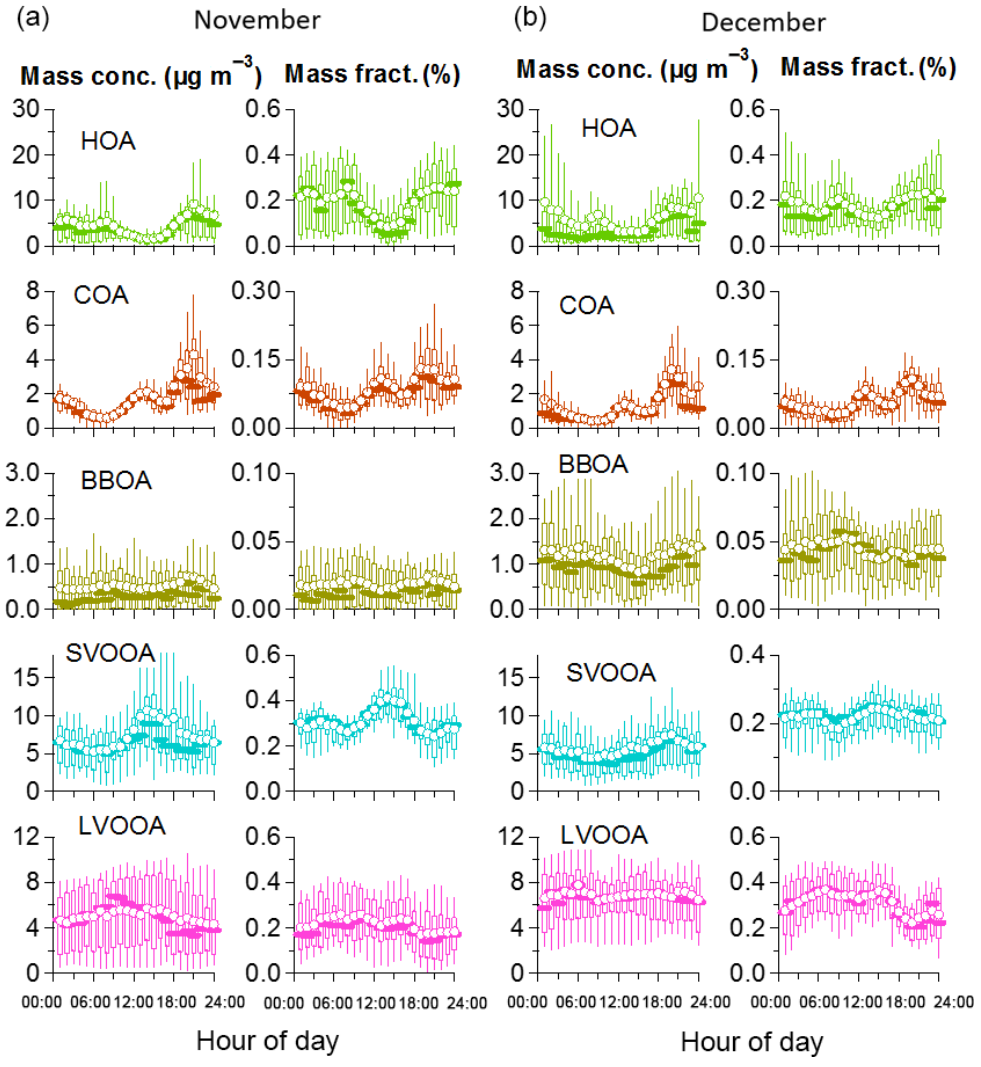

Figure 9. Diurnal variations in ME-2-resolved OA factors during November **(a)** and December **(b)**. Mass concentration of each OA factor (left). Mass fraction of each OA factor (right). 25th- and 75th-percentile boxes, 5th- and 95th-percentile whiskers, median as line in box and mean as solid colored line.

Table 2. Comparison of SOA / O_x average ratios.

Site	Month	Season	SOA–O_x average ratio	Reference
Panyu, Guangzhou	November December	Late autumn Winter	0.23 μg (sm^3 ppb)$^{-1}$* 0.25 μg (sm^3 ppb)$^{-1}$*	This study
Pasadena, CA	May–June (morning) May–June (afternoon)	Late spring–summer Late spring–summer	0.183 μg (sm^3 ppb)$^{-1}$* 0.163 μg (sm^3 ppb)$^{-1}$*	Hayes et al. (2013)
Riverside, CA	July–August	summer	0.142 μg (sm^3 ppb)$^{-1}$*	Docherty et al. (2011)
Mexico City	March	spring	0.156 μg (sm^3 ppb)$^{-1}$*	Aiken et al. (2009)
New York City	July	summer	0.12 μg (m^3 ppb)$^{-1}$	Sun et al. (2011)

* The volume unit "sm" stands for volume under standard-temperature-pressure conditions.

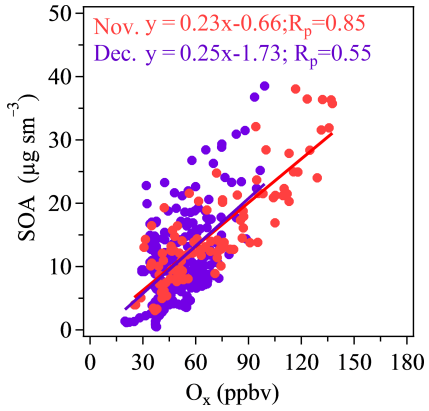

Figure 10. SOA against O_x. The concentration of SOA has been converted to standard-temperature-pressure conditions to compare the slope of SOA / O_x with literature values.

4 Conclusions

In this study, we have found that PM_1 levels in Panyu, a peripheral area of Guangzhou, were significantly affected by traffic emissions. OA were the overwhelmingly dominant species (> 45 %) at all PM_1 levels. A notable increase in the nitrate-to-sulfate ratio was observed with increases in PM concentration, emphasizing the important role of vehicle emission pollutants on high-PM days.

The formation of total nitrate (particulate + gas) was closely correlated with NO_x during both daytime and nighttime with a much steeper slope during daytime than during nighttime. During the day, total nitrate increased as O_x increased at the same NO_x level, suggesting the photochemical formation of nitrate. At night, high total nitrate concentrations were associated with high NO_x but low O_x levels. Ammonium-rich conditions prevailed throughout the campaign, and particulate nitrate was closely associated with excess ammonium. The fraction of particle phase nitrate in December was higher than that in November, primarily due to lower temperatures that favored the partitioning of nitrate toward particle phase.

The nighttime emissions of OA and efficient photochemical production of SOA during the day together accounted for continued high OA concentrations. HOA increased almost linearly with OA concentration and contributed up to 40 % of the high organic concentrations at night. SOA (SVOOA + LVOOA) played a more important role in monthly averages and during the day. SOA concentrations changed with the photochemical oxidation marker (O_x), and the observed ratios of SOA to O_x were higher than those reported for Pasadena and Mexico City during the summer. This efficient SOA formation was fueled by large sources of SOA precursors (e.g., HOA and VOCs) on the periphery of Guangzhou. PM pollution in both megacities and their peripheries should thus be considered together.

Data availability. The data is available upon request. To obtain the data, please contact Chak K. Chan (chak.k.chan@cityu.edu.hk) or Yong Jie Li (yongjieli@umac.mo).

The Supplement related to this article is available online at https://doi.org/10.5194/acp-17-10245-2017-supplement.

Competing interests. The authors declare that they have no conflict of interest.

Acknowledgements. This work was supported by the National Key Project of the Ministry of Science and Technology of the People's Republic of China (2016YFC0201901) and the National Natural Science Foundation of China (41375156). We also thank Dr. Mai Boru for providing CO_2 data. Yi Ming Qin gratefully acknowledges support from the HKUST Asian Future Leaders Scholarship. Chak K. Chan would like to acknowledge the Science Technology and Innovation Committee of Shenzhen municipality (project no. 41675117).

Edited by: Nga Lee Ng
Reviewed by: two anonymous referees

References

Aiken, A. C., DeCarlo, P. F., and Jimenez, J. L.: Elemental analysis of organic species with electron ionization high-resolution mass spectrometry, Anal. Chem., 79, 8350–8358, https://doi.org/10.1021/ac071150w, 2007.

Aiken, A. C., Salcedo, D., Cubison, M. J., Huffman, J. A., DeCarlo, P. F., Ulbrich, I. M., Docherty, K. S., Sueper, D., Kimmel, J. R., Worsnop, D. R., Trimborn, A., Northway, M., Stone, E. A., Schauer, J. J., Volkamer, R. M., Fortner, E., de Foy, B., Wang, J., Laskin, A., Shutthanandan, V., Zheng, J., Zhang, R., Gaffney, J., Marley, N. A., Paredes-Miranda, G., Arnott, W. P., Molina, L. T., Sosa, G., and Jimenez, J. L.: Mexico City aerosol analysis during MILAGRO using high resolution aerosol mass spectrometry at the urban supersite (T0) – Part 1: Fine particle composition and organic source apportionment, Atmos. Chem. Phys., 9, 6633–6653, https://doi.org/10.5194/acp-9-6633-2009, 2009.

Alfarra, M. R., Prevot, A. S. H., Szidat, S., Sandradewi, J., Weimer, S., Lanz, V. A., Schreiber, D., Martin Mohr, A., and Urs, B.: Identification of the Mass Spectral Signature of Organic Aerosols from Wood Burning Emissions, Environ. Sci. Technol., 41, 5770–5777, https://doi.org/10.1021/ES062289B, 2007.

Arimoto, R., Duce, R. A., Savoie, D. L., Prospero, J. M., Talbot, R., Cullen, J. D., Tomza, U., Lewis, N. F., and Ray, B. J.: Relationships among aerosol constituents from Asia and the North Pacific during PEM-West A, J. Geophys. Res., 101, 2011–2023, https://doi.org/10.1029/95JD01071, 1996.

Canagaratna, M. R., Jimenez, J. L., Kroll, J. H., Chen, Q., Kessler, S. H., Massoli, P., Hildebrandt Ruiz, L., Fortner, E., Williams, L. R., Wilson, K. R., Surratt, J. D., Donahue, N. M., Jayne, J. T.,

and Worsnop, D. R.: Elemental ratio measurements of organic compounds using aerosol mass spectrometry: characterization, improved calibration, and implications, Atmos. Chem. Phys., 15, 253–272, https://doi.org/10.5194/acp-15-253-2015, 2015.

Canonaco, F., Crippa, M., Slowik, J. G., Baltensperger, U., and Prévôt, A. S. H.: SoFi, an IGOR-based interface for the efficient use of the generalized multilinear engine (ME-2) for the source apportionment: ME-2 application to aerosol mass spectrometer data, Atmos. Meas. Tech., 6, 3649–3661, https://doi.org/10.5194/amt-6-3649-2013, 2013.

Chan, C. K. and Yao, X.: Air pollution in mega cities in China, Atmos. Environ., 42, 1–42, https://doi.org/10.1016/j.atmosenv.2007.09.003, 2008.

Cheung, H. H. Y., Tan, H., Xu, H., Li, F., Wu, C., Yu, J. Z., and Chan, C. K.: Measurements of non-volatile aerosols with a VTDMA and their correlations with carbonaceous aerosols in Guangzhou, China, Atmos. Chem. Phys., 16, 8431–8446, https://doi.org/10.5194/acp-16-8431-2016, 2016.

Clegg, S. L., Brimblecombe, P., and Wexler, A. S.: Thermodynamic Model of the System H^+–NH_4^+–Na^+–SO_4^{2-}–NO_3^-–Cl^-–H_2O at 298.15 K, J. Phys. Chem. A, 102, 2155–2171, https://doi.org/10.1021/jp973043j, 1998.

Crippa, M., Canonaco, F., Lanz, V. A., Äijälä, M., Allan, J. D., Carbone, S., Capes, G., Ceburnis, D., Dall'Osto, M., Day, D. A., DeCarlo, P. F., Ehn, M., Eriksson, A., Freney, E., Hildebrandt Ruiz, L., Hillamo, R., Jimenez, J. L., Junninen, H., Kiendler-Scharr, A., Kortelainen, A.-M., Kulmala, M., Laaksonen, A., Mensah, A. A., Mohr, C., Nemitz, E., O'Dowd, C., Ovadnevaite, J., Pandis, S. N., Petäjä, T., Poulain, L., Saarikoski, S., Sellegri, K., Swietlicki, E., Tiitta, P., Worsnop, D. R., Baltensperger, U., and Prévôt, A. S. H.: Organic aerosol components derived from 25 AMS data sets across Europe using a consistent ME-2 based source apportionment approach, Atmos. Chem. Phys., 14, 6159–6176, https://doi.org/10.5194/acp-14-6159-2014, 2014.

DeCarlo, P. F., Kimmel, J. R., Trimborn, A., Northway, M. J., Jayne, J. T., Aiken, A. C., Gonin, M., Fuhrer, K., Horvath, T., Docherty, K. S., Worsnop, D. R., and Jimenez, J. L.: Field-Deployable, High-Resolution, Time-of-Flight Aerosol Mass Spectrometer, Anal. Chem., 78, 8281–8289, https://doi.org/10.1021/ac061249n, 2006.

Deng, W., Hu, Q., Liu, T., Wang, X., Zhang, Y., Song, W., Sun, Y., Bi, X., Yu, J., Yang, W., Huang, X., Zhang, Z., Huang, Z., He, Q., Mellouki, A., and George, C.: Primary particulate emissions and secondary organic aerosol (SOA) formation from idling diesel vehicle exhaust in China, Sci. Total Environ., 593, 462–469, https://doi.org/10.1016/j.scitotenv.2017.03.088, 2017.

Docherty, K. S., Aiken, A. C., Huffman, J. A., Ulbrich, I. M., DeCarlo, P. F., Sueper, D., Worsnop, D. R., Snyder, D. C., Peltier, R. E., Weber, R. J., Grover, B. D., Eatough, D. J., Williams, B. J., Goldstein, A. H., Ziemann, P. J., and Jimenez, J. L.: The 2005 Study of Organic Aerosols at Riverside (SOAR-1): instrumental intercomparisons and fine particle composition, Atmos. Chem. Phys., 11, 12387–12420, https://doi.org/10.5194/acp-11-12387-2011, 2011.

Drinovec, L., Močnik, G., Zotter, P., Prévôt, A. S. H., Ruckstuhl, C., Coz, E., Rupakheti, M., Sciare, J., Müller, T., Wiedensohler, A., and Hansen, A. D. A.: The "dual-spot" Aethalometer: an improved measurement of aerosol black carbon with real-time loading compensation, Atmos. Meas. Tech., 8, 1965–1979, https://doi.org/10.5194/amt-8-1965-2015, 2015.

Elser, M., Huang, R.-J., Wolf, R., Slowik, J. G., Wang, Q., Canonaco, F., Li, G., Bozzetti, C., Daellenbach, K. R., Huang, Y., Zhang, R., Li, Z., Cao, J., Baltensperger, U., El-Haddad, I., and Prévôt, A. S. H.: New insights into $PM_{2.5}$ chemical composition and sources in two major cities in China during extreme haze events using aerosol mass spectrometry, Atmos. Chem. Phys., 16, 3207–3225, https://doi.org/10.5194/acp-16-3207-2016, 2016.

Farmer, D. K., Matsunaga, a, Docherty, K. S., Surratt, J. D., Seinfeld, J. H., Ziemann, P. J., and Jimenez, J. L.: Response of an aerosol mass spectrometer to organonitrates and organosulfates and implications for atmospheric chemistry, P. Natl. Acad. Sci. USA, 107, 6670–6675, https://doi.org/10.1073/pnas.0912340107, 2010.

Fröhlich, R., Crenn, V., Setyan, A., Belis, C. A., Canonaco, F., Favez, O., Riffault, V., Slowik, J. G., Aas, W., Aijälä, M., Alastuey, A., Artiñano, B., Bonnaire, N., Bozzetti, C., Bressi, M., Carbone, C., Coz, E., Croteau, P. L., Cubison, M. J., Esser-Gietl, J. K., Green, D. C., Gros, V., Heikkinen, L., Herrmann, H., Jayne, J. T., Lunder, C. R., Minguillón, M. C., Močnik, G., O'Dowd, C. D., Ovadnevaite, J., Petralia, E., Poulain, L., Priestman, M., Ripoll, A., Sarda-Estève, R., Wiedensohler, A., Baltensperger, U., Sciare, J., and Prévôt, A. S. H.: ACTRIS ACSM intercomparison – Part 2: Intercomparison of ME-2 organic source apportionment results from 15 individual, co-located aerosol mass spectrometers, Atmos. Meas. Tech., 8, 2555–2576, https://doi.org/10.5194/amt-8-2555-2015, 2015.

Gentner, D. R., Jathar, S. H., Gordon, T. D., Bahreini, R., Day, D. A., El Haddad, I., Hayes, P. L., Pieber, S. M., Platt, S. M., de Gouw, J., Goldstein, A. H., Harley, R. A., Jimenez, J. L., Prévôt, A. S. H., and Robinson, A. L.: Review of Urban Secondary Organic Aerosol Formation from Gasoline and Diesel Motor Vehicle Emissions, Environ. Sci. Technol., 51, 1074–1093, https://doi.org/10.1021/acs.est.6b04509, 2017.

Gong, Z., Lan, Z., Xue, L., Zeng, L., He, L., and Huang, X.: Characterization of submicron aerosols in the urban outflow of the central Pearl River Delta region of China, Front. Environ. Sci. Eng. China, 6, 725–733, https://doi.org/10.1007/s11783-012-0441-8, 2012.

Griffith, S. M., Huang, X. H. H., Louie, P. K. K., and Yu, J. Z.: Characterizing the thermodynamic and chemical composition factors controlling $PM_{2.5}$ nitrate: Insights gained from two years of online measurements in Hong Kong, Atmos. Environ., 122, 864–875, https://doi.org/10.1016/j.atmosenv.2015.02.009, 2015.

Hayes, P. L., Ortega, a. M., Cubison, M. J., Froyd, K. D., Zhao, Y., Cliff, S. S., Hu, W. W., Toohey, D. W., Flynn, J. H., Lefer, B. L., Grossberg, N., Alvarez, S., Rappenglück, B., Taylor, J. W., Allan, J. D., Holloway, J. S., Gilman, J. B., Kuster, W. C., De Gouw, J. a., Massoli, P., Zhang, X., Liu, J., Weber, R. J., Corrigan, a. L., Russell, L. M., Isaacman, G., Worton, D. R., Kreisberg, N. M., Goldstein, a. H., Thalman, R., Waxman, E. M., Volkamer, R., Lin, Y. H., Surratt, J. D., Kleindienst, T. E., Offenberg, J. H., Dusanter, S., Griffith, S., Stevens, P. S., Brioude, J., Angevine, W. M., and Jimenez, J. L.: Organic aerosol composition and sources in Pasadena, California, during the 2010 CalNex campaign, J. Geophys. Res. Atmos., 118, 9233–9257, https://doi.org/10.1002/jgrd.50530, 2013.

He, L.-Y., Lin, Y., Huang, X.-F., Guo, S., Xue, L., Su, Q., Hu, M., Luan, S.-J., and Zhang, Y.-H.: Characterization of high-resolution aerosol mass spectra of primary organic aerosol emissions from Chinese cooking and biomass burning, Atmos. Chem. Phys., 10, 11535–11543, https://doi.org/10.5194/acp-10-11535-2010, 2010.

He, L.-Y., Huang, X.-F., Xue, L., Hu, M., Lin, Y., Zheng, J., Zhang, R., and Zhang, Y.-H.: Submicron aerosol analysis and organic source apportionment in an urban atmosphere in Pearl River Delta of China using high-resolution aerosol mass spectrometry, J. Geophys. Res., 116, D12304, https://doi.org/10.1029/2010JD014566, 2011.

Ho, K. F., Lee, S. C., Chan, C. K., Yu, J. C., Chow, J. C., and Yao, X. H.: Characterization of chemical species in $PM_{2.5}$ and PM_{10} aerosols in Hong Kong, Atmos. Environ., 37, 31–39, https://doi.org/10.1016/S1352-2310(02)00804-X, 2003.

Hu, W. W., Hu, M., Yuan, B., Jimenez, J. L., Tang, Q., Peng, J. F., Hu, W., Shao, M., Wang, M., Zeng, L. M., Wu, Y. S., Gong, Z. H., Huang, X. F., and He, L. Y.: Insights on organic aerosol aging and the influence of coal combustion at a regional receptor site of central eastern China, Atmos. Chem. Phys., 13, 10095–10112, https://doi.org/10.5194/acp-13-10095-2013, 2013.

Huang, X.-F., He, L.-Y., Hu, M., Canagaratna, M. R., Sun, Y., Zhang, Q., Zhu, T., Xue, L., Zeng, L.-W., Liu, X.-G., Zhang, Y.-H., Jayne, J. T., Ng, N. L., and Worsnop, D. R.: Highly time-resolved chemical characterization of atmospheric submicron particles during 2008 Beijing Olympic Games using an Aerodyne High-Resolution Aerosol Mass Spectrometer, Atmos. Chem. Phys., 10, 8933–8945, https://doi.org/10.5194/acp-10-8933-2010, 2010.

Huang, X., Qiu, R., Chan, C. K. and Ravi Kant, P.: Evidence of high $PM_{2.5}$ strong acidity in ammonia-rich atmosphere of Guangzhou, China: Transition in pathways of ambient ammonia to form aerosol ammonium at $[NH_4^+]/[SO_4^{2-}] = 1.5$, Atmos. Res., 99, 488–495, https://doi.org/10.1016/j.atmosres.2010.11.021, 2011a.

Huang, X.-F., He, L.-Y., Hu, M., Canagaratna, M. R., Kroll, J. H., Ng, N. L., Zhang, Y.-H., Lin, Y., Xue, L., Sun, T.-L., Liu, X.-G., Shao, M., Jayne, J. T., and Worsnop, D. R.: Characterization of submicron aerosols at a rural site in Pearl River Delta of China using an Aerodyne High-Resolution Aerosol Mass Spectrometer, Atmos. Chem. Phys., 11, 1865–1877, https://doi.org/10.5194/acp-11-1865-2011, 2011b.

Jimenez, J. L., Canagaratna, M. R., Donahue, N. M., Prevot, A. S. H., Zhang, Q., Kroll, J. H., DeCarlo, P. F., Allan, J. D., Coe, H., Ng, N. L., Aiken, a C., Docherty, K. S., Ulbrich, I. M., Grieshop, A. P., Robinson, A. L., Duplissy, J., Smith, J. D., Wilson, K. R., Lanz, V. A., Hueglin, C., Sun, Y. L., Tian, J., Laaksonen, a, Raatikainen, T., Rautiainen, J., Vaattovaara, P., Ehn, M., Kulmala, M., Tomlinson, J. M., Collins, D. R., Cubison, M. J., Dunlea, E. J., Huffman, J. A., Onasch, T. B., Alfarra, M. R., Williams, P. I., Bower, K., Kondo, Y., Schneider, J., Drewnick, F., Borrmann, S., Weimer, S., Demerjian, K., Salcedo, D., Cottrell, L., Griffin, R., Takami, A., Miyoshi, T., Hatakeyama, S., Shimono, A., Sun, J. Y., Zhang, Y. M., Dzepina, K., Kimmel, J. R., Sueper, D., Jayne, J. T., Herndon, S. C., Trimborn, A. M., Williams, L. R., Wood, E. C., Middlebrook, A. M., Kolb, C. E., Baltensperger, U., and Worsnop, D. R.: Evolution of organic aerosols in the atmosphere, Science, 326, 1525–1529, https://doi.org/10.1126/science.1180353, 2009.

Kelly, F. J. and Zhu, T.: Transport solutions for cleaner air, Science, 352, 934–936, https://doi.org/10.1126/science.aaf3420, 2016.

Lee, B. P., Li, Y. J., Yu, J. Z., Louie, P. K. K., and Chan, C. K.: Physical and chemical characterization of ambient aerosol by HR-ToF-AMS at a suburban site in Hong Kong during springtime 2011, J. Geophys. Res.-Atmos., 118, 8625–8639, https://doi.org/10.1002/jgrd.50658, 2013.

Lee, B. P., Li, Y. J., Yu, J. Z., Louie, P. K. K., and Chan, C. K.: Characteristics of submicron particulate matter at the urban roadside in downtown Hong Kong – Overview of 4 months of continuous high-resolution aerosol mass spectrometer measurements, J. Geophys. Res.-Atmos., 120, 7040–7058, https://doi.org/10.1002/2015JD023311, 2015.

Li, Y. J., Lee, B. Y. L., Yu, J. Z., Ng, N. L., and Chan, C. K.: Evaluating the degree of oxygenation of organic aerosol during foggy and hazy days in Hong Kong using high-resolution time-of-flight aerosol mass spectrometry (HR-ToF-AMS), Atmos. Chem. Phys., 13, 8739–8753, https://doi.org/10.5194/acp-13-8739-2013, 2013.

Li, Y. J., Sun, Y., Zhang, Q., Li, X., Li, M., Zhou, Z., and Chan, C. K.: Real-time chemical characterization of atmospheric particulate matter in China: A review, Atmos. Environ., 158, 270–304, https://doi.org/10.1016/j.atmosenv.2017.02.027, 2017.

Liu, T., Wang, X., Deng, W., Hu, Q., Ding, X., Zhang, Y., He, Q., Zhang, Z., Lü, S., Bi, X., Chen, J., and Yu, J.: Secondary organic aerosol formation from photochemical aging of light-duty gasoline vehicle exhausts in a smog chamber, Atmos. Chem. Phys., 15, 9049–9062, https://doi.org/10.5194/acp-15-9049-2015, 2015a.

Liu, X., Sun, K., Qu, Y., Hu, M., Sun, Y., Zhang, F., and Zhang, Y.: Secondary formation of sulfate and nitrate during a haze episode in megacity beijing, china, Aerosol Air Qual. Res., 15, 2246–2257, https://doi.org/10.4209/aaqr.2014.12.0321, 2015b.

Louie, P. K. K., Chow, J. C., Chen, L. W. A., Watson, J. G., Leung, G., and Sin, D. W. M.: $PM_{2.5}$ chemical composition in Hong Kong: Urban and regional variations, Sci. Total Environ., 338, 267–281, https://doi.org/10.1016/j.scitotenv.2004.07.021, 2005.

Middlebrook, A. M., Bahreini, R., Jimenez, J. L., and Canagaratna, M. R.: Evaluation of Composition-Dependent Collection Efficiencies for the Aerodyne Aerosol Mass Spectrometer using Field Data, Aerosol Sci. Technol., 46, 258–271, https://doi.org/10.1080/02786826.2011.620041, 2012.

Mohr, C., DeCarlo, P. F., Heringa, M. F., Chirico, R., Slowik, J. G., Richter, R., Reche, C., Alastuey, A., Querol, X., Seco, R., Peñuelas, J., Jiménez, J. L., Crippa, M., Zimmermann, R., Baltensperger, U., and Prévôt, A. S. H.: Identification and quantification of organic aerosol from cooking and other sources in Barcelona using aerosol mass spectrometer data, Atmos. Chem. Phys., 12, 1649–1665, https://doi.org/10.5194/acp-12-1649-2012, 2012.

Paatero, P. and Hopke, P. K.: Rotational tools for factor analytic models, J. Chemom., 23, 91–100, https://doi.org/10.1002/cem.1197, 2009.

Pan, Y., Wang, Y., Zhang, J., Liu, Z., Wang, L., Tian, S., Tang, G., Gao, W., Ji, D., Song, T., and Wang, Y.: Redefining the importance of nitrate during haze pollution to help optimize

an emission control strategy, Atmos. Environ., 141, 197–202, https://doi.org/10.1016/j.atmosenv.2016.06.035, 2016.

Pathak, R. K., Louie, P. K. K., and Chan, C. K.: Characteristics of aerosol acidity in Hong Kong, Atmos. Environ., 38, 2965–2974, https://doi.org/10.1016/j.atmosenv.2004.02.044, 2004.

Platt, S. M., El Haddad, I., Pieber, S. M., Huang, R.-J., Zardini, A. A., Clairotte, M., Suarez-Bertoa, R., Barmet, P., Pfaffenberger, L., Wolf, R., Slowik, J. G., Fuller, S. J., Kalberer, M., Chirico, R., Dommen, J., Astorga, C., Zimmermann, R., Marchand, N., Hellebust, S., Temime-Roussel, B., Baltensperger, U., and Prévôt, A. S. H.: Two-stroke scooters are a dominant source of air pollution in many cities, Nat. Commun., 5, 3749, https://doi.org/10.1038/ncomms4749, 2014.

Qin, Y. M., Li, Y. J., Wang, H., Lee, B. P. Y. L., Huang, D. D., and Chan, C. K.: Particulate matter (PM) episodes at a suburban site in Hong Kong: evolution of PM characteristics and role of photochemistry in secondary aerosol formation, Atmos. Chem. Phys., 16, 14131–14145, https://doi.org/10.5194/acp-16-14131-2016, 2016.

Schneider, J., Weimer, S., Drewnick, F., Borrmann, S., Helas, G., Gwaze, P., Schmid, O., Andreae, M. O., and Kirchner, U.: Mass spectrometric analysis and aerodynamic properties of various types of combustion-related aerosol particles, Int. J. Mass Spectrom., 258, 37–49, https://doi.org/10.1016/j.ijms.2006.07.008, 2006.

Schurman, M. I., Lee, T., Desyaterik, Y., Schichtel, B. A., Kreidenweis, S. M., and Collett, J. L.: Transport, biomass burning, and in-situ formation contribute to fine particle concentrations at a remote site near Grand Teton National Park, Atmos. Environ., 112, 257–268, https://doi.org/10.1016/j.atmosenv.2015.04.043, 2015.

Seinfeld, J. H. and Pandis, S. N.: Atmospheric From Air Pollution to Climate Change, 2nd Edn., Wiley, New Jersey, 2006.

Sun, Y.-L., Zhang, Q., Schwab, J. J., Demerjian, K. L., Chen, W.-N., Bae, M.-S., Hung, H.-M., Hogrefe, O., Frank, B., Rattigan, O. V., and Lin, Y.-C.: Characterization of the sources and processes of organic and inorganic aerosols in New York city with a high-resolution time-of-flight aerosol mass apectrometer, Atmos. Chem. Phys., 11, 1581–1602, https://doi.org/10.5194/acp-11-1581-2011, 2011.

Tan, H., Yin, Y., Gu, X., Li, F., Chan, P. W., Xu, H., Deng, X., and Wan, Q.: An observational study of the hygroscopic properties of aerosols over the Pearl River Delta region, Atmos. Environ., 77, 817–826, https://doi.org/10.1016/j.atmosenv.2013.05.049, 2013.

Tan, J.-H., Duan, J.-C., Chen, D.-H., Wang, X.-H., Guo, S.-J., Bi, X.-H., Sheng, G.-Y., He, K.-B., and Fu, J.-M.: Chemical characteristics of haze during summer and winter in Guangzhou, Atmos. Res., 94, 238–245, https://doi.org/10.1016/j.atmosres.2009.05.016, 2009.

Wang, Y., Zhang, Q. Q., He, K., Zhang, Q., and Chai, L.: Sulfate-nitrate-ammonium aerosols over China: response to 2000–2015 emission changes of sulfur dioxide, nitrogen oxides, and ammonia, Atmos. Chem. Phys., 13, 2635–2652, https://doi.org/10.5194/acp-13-2635-2013, 2013.

Wen, L., Chen, J., Yang, L., Wang, X., Xu, C., Sui, X., Yao, L., Zhu, Y., Zhang, J., Zhu, T., and Wang, W.: Enhanced formation of fine particulate nitrate at a rural site on the North China Plain in summer: The important roles of ammonia and ozone, Atmos. Environ., 101, 294–302, https://doi.org/10.1016/j.atmosenv.2014.11.037, 2015.

Wu, X., Wu, Y., Zhang, S., Liu, H., Fu, L., and Hao, J.: Assessment of vehicle emission programs in China during 1998–2013: Achievement, challenges and implications, Environ. Pollut., 214, 556–567, https://doi.org/10.1016/j.envpol.2016.04.042, 2016.

Xu, L., Suresh, S., Guo, H., Weber, R. J., and Ng, N. L.: Aerosol characterization over the southeastern United States using high-resolution aerosol mass spectrometry: spatial and seasonal variation of aerosol composition and sources with a focus on organic nitrates, Atmos. Chem. Phys., 15, 7307–7336, https://doi.org/10.5194/acp-15-7307-2015, 2015.

Xue, J., Yuan, Z., Lau, A. K. H., and Yu, J. Z.: Insights into factors affecting nitrate in $PM_{2.5}$ in a polluted high NO_x environment through hourly observations and size distribution measurements, J. Geophys. Res. Atmos., 119, 4888–4902, https://doi.org/10.1002/2013JD021108, 2014.

Zhang, Q., Jimenez, J. L., Canagaratna, M. R., Ulbrich, I. M., Ng, N. L., Worsnop, D. R., and Sun, Y.: Understanding atmospheric organic aerosols via factor analysis of aerosol mass spectrometry: A review, Anal. Bioanal. Chem., 401, 3045–3067, https://doi.org/10.1007/s00216-011-5355-y, 2011.

Zhang, Q., Geng, G. N., Wang, S. W., Richter, A., and He, K. Bin: Satellite remote sensing of changes in NO_x emissions over China during 1996–2010, Chinese Sci. Bull., 57, 2857–2864, https://doi.org/10.1007/s11434-012-5015-4, 2012.

Zhang, R., Wang, G., Guo, S., Zamora, M. L., Ying, Q., Lin, Y., Wang, W., Hu, M., and Wang, Y.: Formation of Urban Fine Particulate Matter, Chem. Rev., 115, 3803–3855, https://doi.org/10.1021/acs.chemrev.5b00067, 2015.

Zhang, Y., Sun, J., Zhang, X., Shen, X., Wang, T., and Qin, M.: Seasonal characterization of components and size distributions for submicron aerosols in Beijing, Sci. China Earth Sci., 56, 890–900, https://doi.org/10.1007/s11430-012-4515-z, 2013.

Zhang, Y., Cai, J., Wang, S., He, K., and Zheng, M.: Review of receptor-based source apportionment research of fine particulate matter and its challenges in China, Sci. Total Environ., 586, 917–929, https://doi.org/10.1016/j.scitotenv.2017.02.071, 2017.

Zhang, Y.-L. and Cao, F.: Fine particulate matter ($PM_{2.5}$) in China at a city level., Sci. Rep., 5, 14884, https://doi.org/10.1038/srep14884, 2015.

Zotter, P., El-haddad, I., Zhang, Y., Hayes, P. L., Zhang, X., Lin, Y.-H., Wacker, L., Schnelle-Kreis, J., Abbaszade, G., Zimmermann, R., Surratt, J. D., Weber, R., Jimenez, J. L., Szidat, S., Baltensperger, U., and Prévôt, A. S. H.: Diurnal cycle of fossil and nonfossil carbon using radiocarbon analyses during CalNex, J. Geophys. Res.-Atmos., 119, 6818–6835, https://doi.org/10.1002/2013JD021114, 2014.

Zou, Y., Deng, X. J., Zhu, D., Gong, D. C., Wang, H., Li, F., Tan, H. B., Deng, T., Mai, B. R., Liu, X. T., and Wang, B. G.: Characteristics of 1 year of observational data of VOCs, NO_x and O_3 at a suburban site in Guangzhou, China, Atmos. Chem. Phys., 15, 6625–6636, https://doi.org/10.5194/acp-15-6625-2015, 2015.